

Chapter 1

Introduction

This chapter gives a brief introduction to the self-assembly of amphiphilic molecules and the experimental techniques used to identify their organization in aqueous solutions. Section 1.1 describes the thermodynamics of self-assembly of amphiphilic molecules. Their general phase behaviour is discussed in section 1.2. In the next section, the effects of various additives on their phase behaviour is outlined. Section 2 contains the basic theory of x-ray diffraction and a brief description of the experimental set up used for studying lyotropic liquid crystalline phases. The principles of polarizing optical microscopy is discussed in section 3. The characterization of different liquid crystalline phases using optical polarizing microscopy and x-ray diffraction is described in the last section.

1.1 Amphiphiles

Amphiphilic molecules are made up of two parts of opposing nature: one is a hydrophilic part referred to as the ‘head’ group and other is a hydrophobic ‘tail’ group. The non-polar tail part is usually a long hydrocarbon chain which is covalently attached to the polar head group. Amphiphilic molecules are classified depending on the nature of their head groups. The head groups of ionic amphiphiles dissociate in aqueous solutions and acquire an electric charge. For example, cetyltrimethylammonium bromide (CTAB) is a cationic surfactant and sodium dodecylsulfate (SDS) is an anionic surfactant (Fig. 1.1). The nonionic surfactant *n*-dodecyl tetra (ethylene oxide) ($C_{12}E_4$) does not contain any charge but its head group is polar (Fig. 1.2A). There is another kind of amphiphilic molecules which is known as zwitterionic. The head groups of these molecules

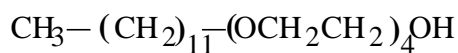


Figure 1.1: Chemical structure of (A) cationic surfactant cetyltrimethylammonium bromide (CTAB) and (B) anionic surfactant sodium dodecylsulfate.

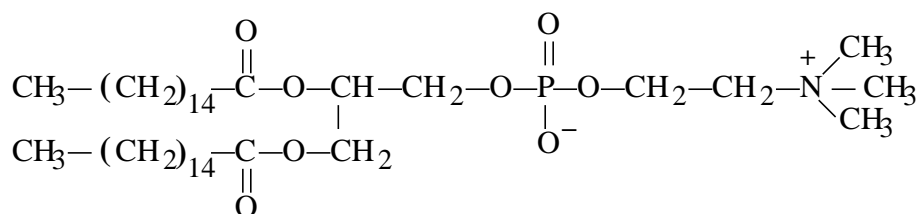
acquire a dipole moment in aqueous solutions. Dipalmitoyl phosphatidylcholine (DPPC) is an example of such an amphiphile (Fig. 1.2B). Synthetic amphiphilic molecules are often referred to as surfactants (short for surface active agents), whereas amphiphiles of biological origin are called lipids.

Strongly hydrated ions and zwitterions have high water solubility and repel each other strongly in water. These molecules along with some uncharged and even non-polar molecules with right geometry and containing electronegative atoms capable of associating with the hydrogen bond network of water are known as hydrophilic molecules. These molecules have the effect of disordering the water molecules around them which ultimately increases the entropy of the system and favours the molecules to be in contact with water [1]. There is another category of molecules, that includes hydrocarbons and fluorocarbons, which do not like to be in contact with water and are known as hydrophobic molecules. The water molecules close to such nonpolar molecule form a ‘cage’ around it. In bulk liquid each water molecule on an average forms 3.0 to 3.5 H bonds with neighboring molecules, whereas in the cage-like structure the number of H bonds is higher (~ 4). These water molecules, therefore, are more ordered than those in the bulk liquid. Thus the reorientation or restructuring of the water molecules around the nonpolar molecule is entropically unfavourable. Although the origin of hydrophobicity is still under debate, the explanation mentioned above is the one commonly discussed in the literature [1, 2].

There are many industrial applications of amphiphilic molecules among which their use for cleansing (soaps and detergents) is one of the oldest [3]. They are very important in cosmetics and oil industry. Viscoelastic solutions of amphiphiles are widely used as lubricants. Their potential use in pharmaceutical industry for drug delivery has attracted a lot of attention recently. Stacks of layers of these molecules, called Langmuir-Blodgett films, are important in developing new optical



A



B

Figure 1.2: Chemical structure of (A) nonionic surfactant *n*-dodecyl tetra (ethylene oxide) ($C_{12}E_4$) and (B) zwitterionic lipid dipalmitoyl phosphatidylcholine (DPPC).

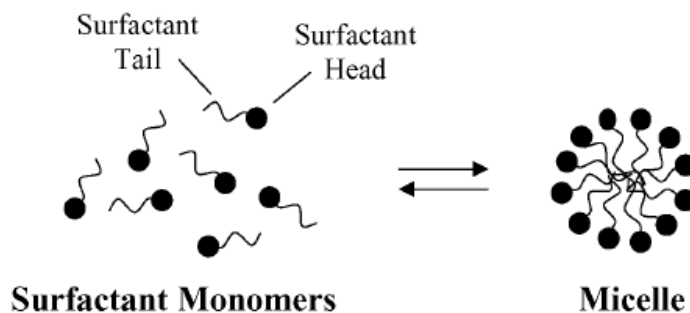


Figure 1.3: Schematic of reversible monomer-micelle thermodynamic equilibrium. The black circles and the curved lines are surfactant ‘heads’ and ‘tails’, respectively.

and electronic devices. The bilayer structure of biological membranes in living cells has inspired many biophysicists to study bilayers of simple amphiphilic molecules as model membranes. The recent development of nanotechnology has again expanded their field of application. For example, various liquid crystalline phases exhibited by these molecules have been used as templates for the synthesis of mesoporous materials and nano particles. Some of these phases have also been used for protein crystallization [4] and as substrates for NMR study of biomolecules.

1.1.1 Self assembly of amphiphilic molecules

At very low concentrations amphiphiles are found to form a monolayer at the air-water interface. In these layers the hydrophilic part of the molecules get anchored to the water surface whereas

the hydrophobic part stays away from water. On increasing the concentration the monolayer gets saturated and the amphiphiles form aggregates in water, such that their hydrophobic parts are screened from the water molecules by their hydrophilic parts. This phenomenon is referred to as self-assembly and the aggregates formed are called micelles. The amphiphile concentration at which self-assembly occurs is called the critical micellar concentration (CMC). Below CMC the amphiphiles are dispersed in water as monomers, whereas above CMC micelles coexist with monomers. Not all amphiphiles form micelles; this is due mainly to their inability to pack into aggregates where their hydrophobic parts are sufficiently screened from water.

The phenomenon of self-assembly can be understood using basic concepts of thermodynamics of ideal solutions. Since CMC is typically of the order of mM or lower, the system can be considered as a multicomponent ideal solution, where aggregates of a given size constitutes one component. The size of an aggregate can be specified in terms of an aggregation number, which is the number of amphiphiles in the aggregate. Thermodynamic equilibrium requires amphiphile in the solution to have same chemical potential (Fig. 1.3). It has two contributions: first one is the reference chemical potential arising from the mean interaction free energy per molecule (μ_N^0) and the other one comes from the entropy of mixing. Therefore, the average chemical potential per amphiphile in an N-mer can be written as [1, 3],

$$\mu_N = \mu_N^0 + \frac{k_B T}{N} \log \frac{X_N}{N} \quad (1.1)$$

where μ_N is the mean chemical potential of an amphiphile in an aggregate of aggregation number N and X_N the concentration of amphiphiles in such aggregates. k_B is the Boltzmann constant. From the conservation relation for the total amphiphile concentration (X),

$$\sum_N X_N = X \quad (1.2)$$

Equating μ_N to μ_1 we get,

$$X_N = N \{X_1 \exp[(\mu_1^0 - \mu_N^0)/k_B T]\}^N \quad (1.3)$$

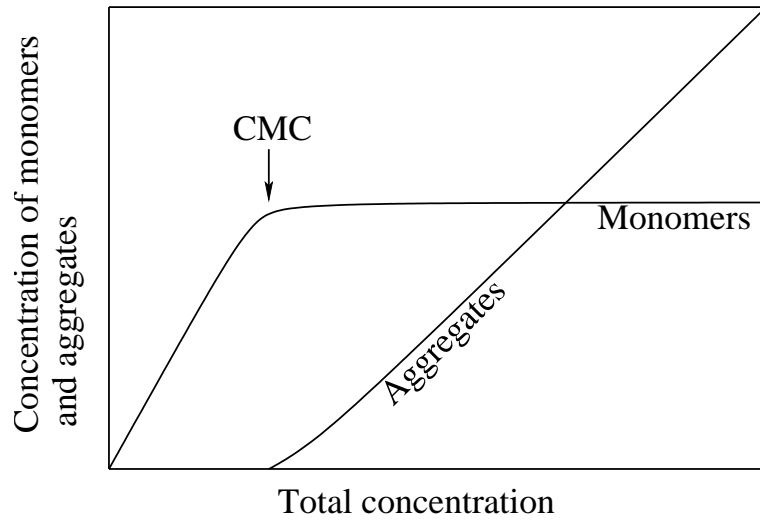


Figure 1.4: Monomer and aggregate concentrations as a function of total amphiphile concentration.

From this equation, it follows that aggregation takes place when the energy per amphiphile in the aggregate is less than that of a monomer i.e., $\mu_N^0 < \mu_1^0$. When the monomer concentration X_1 is very low, such that $X_1 \exp[(\mu_1^0 - \mu_N^0)/k_B T]$ is much less than unity, we have $X_1 \gg X_2 \gg X_3$, etc. Thus, all the amphiphiles will be in the monomer form in this dilute regime. As the amphiphile concentration X is increased, the above equation indicates that X_1 reaches a saturation value less than unity; else X_N will grow without bound for large N , and the condition that $X = \sum_N X_N \ll 1$ (dilute solution) cannot be satisfied. This limiting value of X_1 is given by,

$$X_1 = \exp[-(\mu_1^0 - \mu_N^0)/k_B T]. \quad (1.4)$$

This maximum monomer concentration can be identified as the critical micellar concentration (CMC) and further increase in X leads to the formation of aggregates (Fig. 1.4). For example, CMC of CTAB $\sim 10^{-3}M$, whereas for the lipid DPPC it is $\sim 10^{-12}M$. There are many factors which influence the value of CMC, such as the length of the hydrocarbon chain of the amphiphile, temperature, pressure and added salts [5].

1.1.2 Shape of aggregates

The micelles formed by many of the amphiphiles just above CMC are spherical in shape. At slightly higher concentrations three different shapes are usually observed- spheres, cylinders and

$p = v/(a_o l_c)$	shape	aggregate
$< 1/3$	cone	spherical micelle
$1/3 - 1/2$	truncated cone	cylindrical micelle
~ 1	cylinder	planer bilayer
> 1	inverted truncated cone	inverted micelle

Table 1.1: The packing parameter and different aggregates of amphiphilic molecules.

bilayers. These shapes in very dilute solutions, where inter-micellar interactions are negligible, can be interpreted in terms of the geometrical shape of the individual molecules. The *packing parameter* or *shape parameter* of an amphiphile can be defined as,

$$p = \frac{v}{a_o l_c} \quad (1.5)$$

where a_o is the optimal head group area, v the hydrocarbon chain volume and l_c the chain length. For $p < 1/3$, the molecules have a conical shape, which would force the aggregate to have a spherical shape. For other values of this parameter (Table 1.1), the molecules can form cylindrical micelles, planer bilayer or inverted micelles (Fig. 1.5). However the aggregate structure of a given amphiphile is a function of temperature and of the solution conditions, such as ionic strength and concentration.

In the case of a spherical micelle the local environment of all the amphiphiles is similar, and the radius of the micelle is determined by the length of the hydrocarbon chain of the amphiphile. This results in the aggregates being almost monodisperse in their size distribution. The radius of a cylindrical micelle is again set by the length of the amphiphile. These cylindrical micelles have hemispherical end-caps, which cost additional energy to create. This end-cap energy is clearly independent of the length of the cylinder. The length distribution of cylindrical micelles is determined by the competition between entropy, which would favour shorter and hence larger number of micelles, and end-cap energy, which would favour longer and hence smaller number of micelles. Since the end-cap energy is independent of the length of the cylinder, this results in a very broad length distribution of these micelles. Disc-like micelles are generally unstable and coalesce to form an infinite bilayer in order to decrease the edge energy, which depends on the perimeter of the disc.

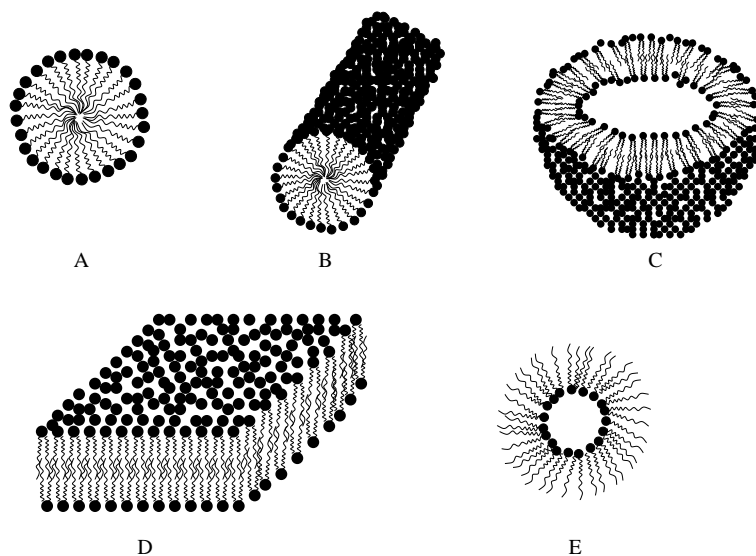


Figure 1.5: Various self assembled structures of amphiphilic molecules : (A) spherical micelle, (B) cylindrical micelle, (C) vesicle, (D) bilayer and (E) inverted micelle. In all these structures, the molecules expose their hydrophilic head group to water and shield their hydrophobic tail from water.

Under certain circumstances, a bilayer can curl up and form closed shell vesicles. Some dilute amphiphilic systems are known to produce fairly monodisperse vesicles, whose origin is still not well understood. Although disc-like micelles are in general unstable, stable micelles of this type are found in some amphiphilic systems. Very often these are effectively binary amphiphilic systems, and the disc-like aggregates are stabilized by a partial phase separation of the two components within each micelle.

1.1.3 Phase behaviour of amphiphilic molecules

Just above CMC amphiphiles in general form an isotropic dispersion of spherical micelles. On increasing the concentration single-chained surfactants such as CTAB shows a transition from spherical to cylindrical micelles, which are randomly distributed both in position and orientation. At higher concentrations, these cylindrical micelles might exhibit a nematic (N) phase with long-range orientational order and short-range positional order [6, 7]. The direction of preferred orientation is denoted by a unit vector called the ‘nematic director’ (Fig. 1.6A). At still higher concentrations the cylindrical micelles arrange on a two dimensional (2-D) hexagonal lattice, with their long axes normal to the plane of the lattice (Fig. 1.6B). Such a hexagonal phase (H_I) is usu-

ally observed over a wide range of surfactant concentration ($\sim 30 - 60$ wt%). Further increase of concentration transforms the hexagonal phase to a lamellar phase (L_α), consisting of a periodic stack of bilayers (Fig. 1.6C). This phase can be looked at as a one dimensional (1-D) lattice of bilayers, with liquid-like positional ordering of the molecules within the bilayers. Further increase of concentration in some systems leads to a hexagonal phase made up of inverse cylindrical micelles (H_{II}). The general phase behaviour of surfactant-water system is schematically illustrated in figure 1.7. The *Kraft temperature* shown in the figure is the temperature below which the amphiphile is in the crystalline phase and is insoluble in water.

Double-chained lipids, such as DPPC, form only bilayers at all concentrations. Hence these amphiphiles exhibit only lamellar phases. In these systems the fluid L_α phase forms above a chain melting transition temperature, above which the hydrocarbon chains of the lipids are in a molten state. At lower temperatures a lamellar ‘gel’ phase is formed, where the hydrocarbon chains are mainly in the all-*trans* conformation and arranged on a 2-D lattice within each bilayer. However, the lattices in adjacent bilayers are not correlated.

The nematic, hexagonal and lamellar phases described above have symmetry properties intermediate between those of an isotropic liquid and a crystal, and are known as liquid crystalline phases or mesophases [6]. The liquid crystalline phases of amphiphiles are referred to as lyotropic liquid crystals, since they form in the presence of a solvent. Liquid crystalline phases are also exhibited by some molecular crystals on heating; these are referred to as thermotropic liquid crystals. It should be noted that lyotropic systems may also exhibit phase transitions on changing the temperature.

The sequence of phases of amphiphilic-water system described above - isotropic, hexagonal and lamellar - has been well known for many years. Detailed phase diagram studies have more recently shown that a variety of phases can occur over a rather narrow composition range between the hexagonal and lamellar phases. The transition from the 2-D hexagonal to 1-D lamellar phase is accompanied by a change from cylindrical micelles with positive interfacial curvature to bilayers with zero interfacial curvature. Frequently bicontinuous cubic phases, which are optically isotropic, have been identified between the hexagonal and lamellar phases [8, 9, 10]. In this phase

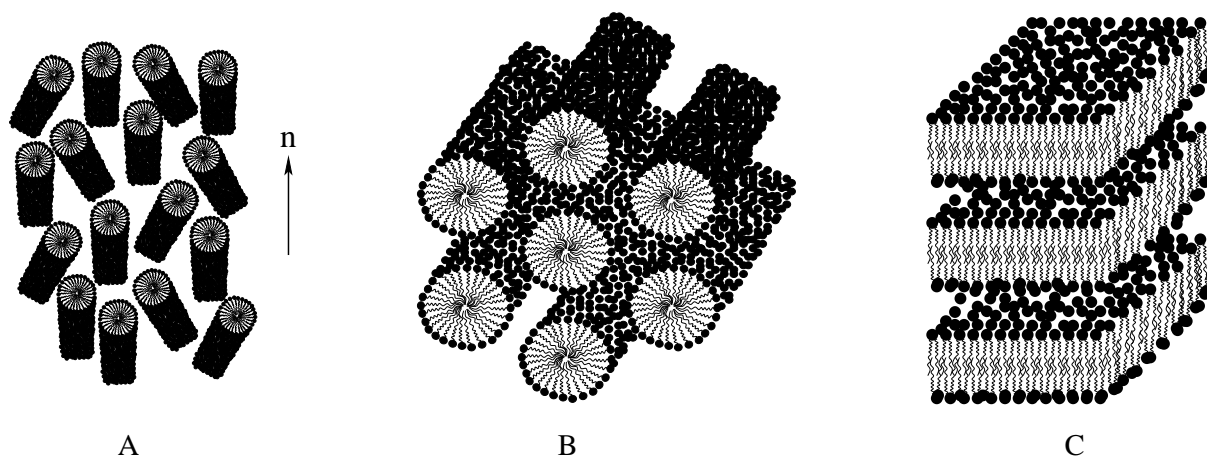


Figure 1.6: Schematics of various lyotropic liquid crystalline phases: (A) nematic phase of rod-like micelles (N_c), (B) 2-D hexagonal phase (H_I) and (C) lamellar phase (L_α).

the amphiphiles form a bilayer that spans the entire sample which separates two interpenetrating water regions. The mid-plane of the bilayer describes a minimal surface with vanishing mean curvature at each point. In addition, some birefringent phases have also been occasionally observed in this composition range and are known as ‘intermediate phases’ [10, 11, 12]. Ribbon phases are the most comprehensively studied intermediate phases which are made up of long flat ribbons with an aspect ratio of ~ 0.5 . They are found to arrange on 2-D lattices of oblique or rectangular symmetry. There are other intermediate phases with layered mesh structure. Two types of mesh phases have been identified. The random mesh phase is a lamellar phase, where each layer is a mesh-like aggregate; there are no positional correlations of the in-plane structure across the layers. In the intermediate ordered mesh phase the mesh-like layers are stacked in a regular fashion, so that this phase is described by a three dimensional (3-D) lattice. A system has been reported, which shows a cubic phase corresponding to space group $Ia\bar{3}d$ on heating and a mesh phase with rhombohedral symmetry ($R\bar{3}m$) on cooling over a narrow composition range between the hexagonal and lamellar phases [13].

Hyde has constructed a catalogue of surfaces that can occur in surfactant-water systems based on some general considerations [14, 15]. He has also classified them according to their topology and has related the global interfacial geometry to the local molecular shape described by the parameter $p = v/a_0l$, discussed earlier. According to this model, mesh-like aggregates (Fig. 1.8A) are

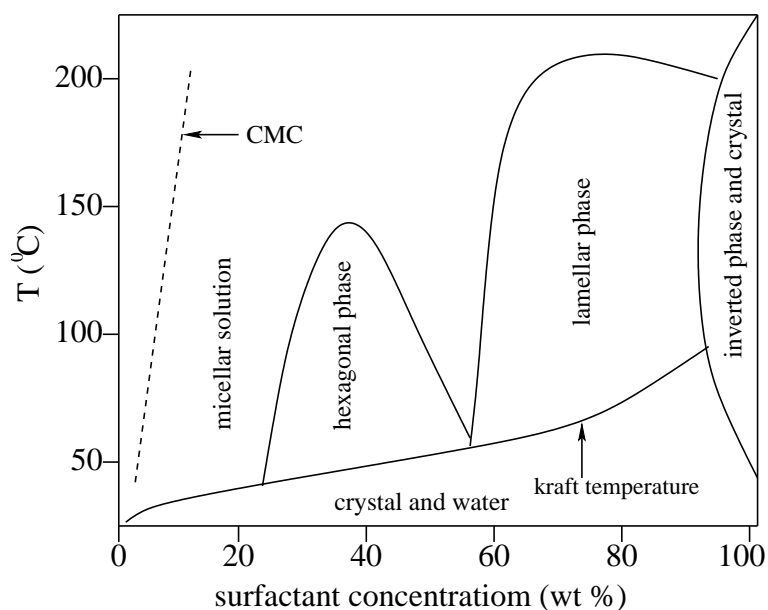


Figure 1.7: Typical phase diagram of an amphiphile-water system.

preferred for $1/2 < p < 2/3$, whereas infinite periodic minimal surfaces (Fig. 1.8B) corresponding to bicontinuous cubic phases can be obtained for higher values of p .

Holmes and his co-workers have studied various bicontinuous and intermediate mesh phases in nonionic surfactant systems. For the C_nEO_m surfactants, it is observed that the shorter homologue ($n \sim 12$) forms bicontinuous cubic phase between the hexagonal and lamellar phases [16]. On increasing the chain length the cubic phase appears only in a very narrow range of surfactant concentration. Here a lamellar phase with water filled curvature defects is found over an extensive region between hexagonal and lamellar phases [12, 17]. Further increase of chain length ($n \sim 30$) completely replaces the cubic phase by a mesh phase [18]. The structures of both these bicontinuous and mesh phases are consistent with the theoretical predictions of Hyde discussed above. However the theory does not explain the role of chain length in determining the structure. It has been conjectured that the increase in micellar curvature due to an increase in the head group size gives rise to the cubic phase, whereas the decrease in the flexibility of the aggregate due to an increase in the chain length induces the intermediate mesh phase. The bicontinuous cubic phase may have different symmetry corresponding to different space groups, such as $Ia3d$, $Pn3m$ and $Im3m$ [19]. On the other hand, most frequently observed mesh phases have two different structures: one

consists of a 2-D square mesh where four rods meet at each nodal point, the other is a hexagonal mesh, where three rods meet at each nodal point.

1.1.4 Influence of additives on the phase behaviour of amphiphile-water systems

The physical properties of amphiphile-water systems are very sensitive to the nature of additives. The most common additives in ionic amphiphilic systems are inorganic salts, such as NaCl and KBr. The addition of *KBr* to a dilute solution of the cationic surfactant, CTAB, makes the cylindrical micelles to elongate into very long worm-like micelles. There have been many studies of the dramatic changes in the viscoelastic properties of such systems due to the entanglement of the worm-like micelles [20, 21]. These systems have very interesting similarities with polymer solutions and have been the subject of many theoretical and experimental investigations [22]. It is observed that organic salts are highly efficient in promoting such micellar growth at significantly low salt concentrations. The addition of sodium salicylate (SS) to a CTAB solution has been shown to result in entangled worm-like micelles, with the persistence length (which is the length scale over which the micelle can be treated as rigid) ranging from 100 to 200 *nm*. Similar observations have also been reported in the anionic surfactant sodium dodecylsulfate (SDS) in the presence of *p*-toluidine hydrochloride (PTHC) [23]. The growth of the micelles in the presence of these salts can be attributed to a decrease in the end-cap energy of the micelles; the system reacts by reducing the number of end caps, and hence by increasing the average length of the micelles. The addition of a salt, such as SS, to CTAB introduces a new counterion for the cationic amphiphile. Since the salicylate ion is hydrophobic in nature, it will have a tendency to bind strongly to the micelle. NMR studies have shown similar counterions to bind strongly to the surface of surfactant micelles by inserting their hydrophobic moiety into the hydrocarbon region of the micelle [23, 24] (Fig. 1.9). One extreme limit of an embedded counterion is an oppositely charged surfactant. Aqueous solutions of mixtures of anionic and cationic surfactants are known to show interesting properties, such as low critical micellar concentration (CMC), high surface activity, formation of liquid crystalline phases at higher water content and spontaneous formation of vesicles [25, 26, 27, 28].

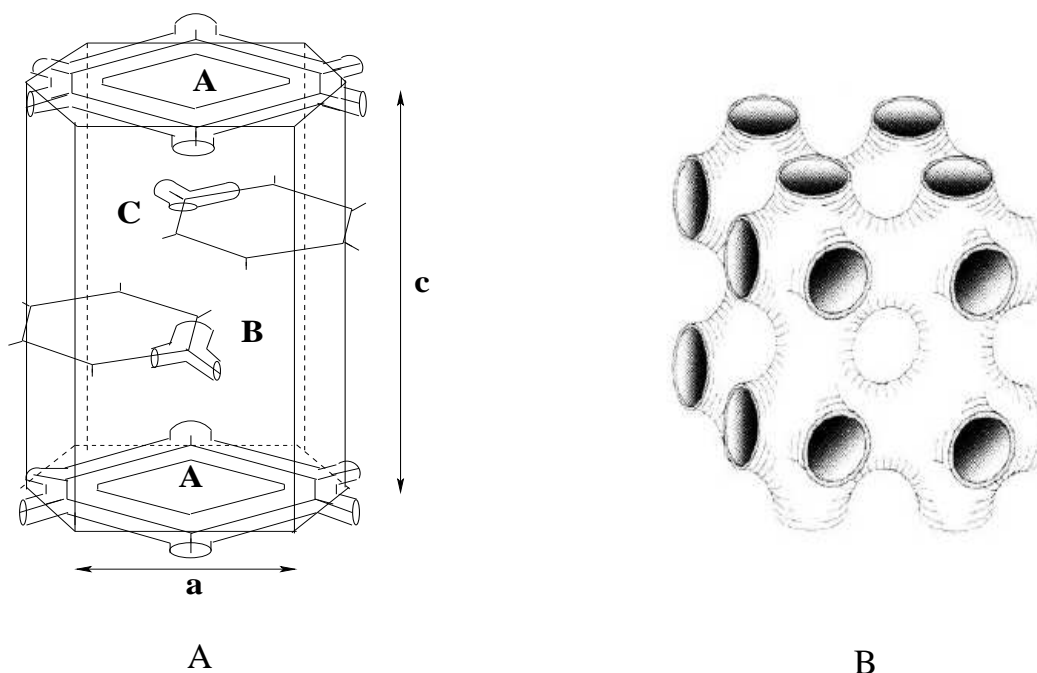


Figure 1.8: Schematic of (A) an ordered mesh phase and (B) a bicontinuous cubic phase, respectively.

However, almost all these investigations have been confined to dilute solutions with surfactant concentrations ≤ 5 wt%.

The bending rigidity (κ) of lipid bilayers is typically an order of magnitude larger than the thermal energy $k_B T$. It is well known that by using short chain alcohols as a co-surfactant κ can be made comparable to $k_B T$. Alcohols are also known to induce worm-like micelles in some amphiphilic systems. Simple inorganic salts have strong influence on interbilayer interactions both in neutral and charged lipid systems [29]. The swollen lamellar phase of neutral amphiphiles, with intermembrane spacings ~ 100 nm, is found to be stabilized by thermal undulations of the bilayers. The addition of a trace of ionic surfactant to such a system suppresses the thermal undulations leading to a substantial reduction in the lamellar periodicity [30]. Addition of small hydrophobic molecules to didodecyldimethylammonium bromide (DDAB) has been shown to induce cubic phases corresponding to different space groups [19]. In all these cases, the interaggregate interactions and the aggregate flexibility are affected by the presence of such additives.

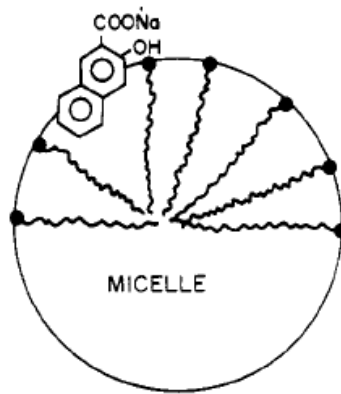


Figure 1.9: Schematic of the orientation of an organic counterion at the micellar surface [24].

1.2 X-ray diffraction

1.2.1 Theory of x-ray diffraction

X-rays are electromagnetic radiation with wave length in the range ($\sim 0.1 - 100 \text{ \AA}$) lying between ultraviolet (UV) and gamma radiation. The oscillating electric field of this radiation exerts a force on the electrons of the atom in the scattering medium. According to classical electromagnetic theory, these accelerated charges radiate. This scattered radiation, which has the same frequency as the incident radiation, spreads out in all directions from the atom in the form of a spherical wave. The scattered radiation from the different atoms interfere to produce the diffraction pattern, which, therefore, depends on the electron density distribution in the scattering medium [31].

Consider a monochromatic planar wave incident on a point scatterer, such as an electron, sitting at the origin. It can be expressed as [32],

$$\Phi_{in} = \Phi_o e^{i\vec{k}_o \cdot \vec{r}} \quad (1.6)$$

where Φ_o is the amplitude of the plane wave and \vec{k}_o its wave vector. The amplitude of the scattered spherical wave at a distance R can be written as,

$$\Phi_{sc} = \frac{\Phi_o A}{R} e^{ikR} \quad (1.7)$$

where A is the ‘scattering length’, which determines the strength of scattering. Now consider another electron at a distance \vec{r} from the first one (Fig. 1.10). The phase difference between the

rays scattered by the two electrons can be expressed as $(\vec{k} - \vec{k}_o) \cdot \vec{r}$ where \vec{k} is the wave vector in the direction of scattering. $\vec{q} = \vec{k} - \vec{k}_o$ is known as the scattering vector and its magnitude is given by $|\vec{q}| = (4\pi \sin\theta)/\lambda$, where 2θ is the scattering angle between \vec{k} and \vec{k}_o . The amplitude of the scattered wave at R ($\gg r$) where the scattered rays can be treated as parallel is given by,

$$\Phi_{sc} = \frac{\Phi_o a}{R} e^{i(kR - \vec{q} \cdot \vec{r})} \quad (1.8)$$

For an assembly of N scatterers at \vec{r}_i ($i = 1, 2, 3, \dots, N$), the above expression can be summed up to get the total amplitude of the scattered beam.

$$\Phi_{tot} = \frac{\Phi_o a}{R} e^{ikR} \sum_{i=1}^N e^{-i\vec{q} \cdot \vec{r}_i} \quad (1.9)$$

For a material of electron density $\rho(\vec{r}) = \sum \delta(\vec{r} - \vec{r}_i)$, the above equation can be modified to,

$$\Phi_{tot} = \frac{\Phi_o a}{R} e^{ikR} \int \rho(\vec{r}) e^{-i\vec{q} \cdot \vec{r}} d\vec{r} \quad (1.10)$$

This expression shows that the amplitude of the scattered wave is proportional to the Fourier transform of the electron density function of the scattering medium. The expression is derived based on the assumption that multiple scattering from the medium is negligible. The intensity of scattered radiation is the square of its amplitude and hence is given by,

$$I(\vec{q}) = |\Phi_{tot}|^2 = \left| \frac{\Phi_o a}{R} e^{ikR} \int \rho(\vec{r}) e^{-i\vec{q} \cdot \vec{r}} d\vec{r} \right|^2 \quad (1.11)$$

In the following chapters of this thesis x-ray diffraction technique has been used to identify various lyotropic liquid crystalline phases. For such periodic structures, the electron density $\rho(\vec{r})$ can be written as the convolution of a lattice function $\rho_l(\vec{r})$, describing the periodic lattice, and a basis function $\rho_b(\vec{r})$, describing the electron density within each unit cell.

$$\rho(\vec{r}) = \rho_l(\vec{r}) \otimes \rho_b(\vec{r}) \quad (1.12)$$

Since the Fourier transform of the convolution of two functions is the product of their Fourier transforms, from Eq. (1.12) we get,

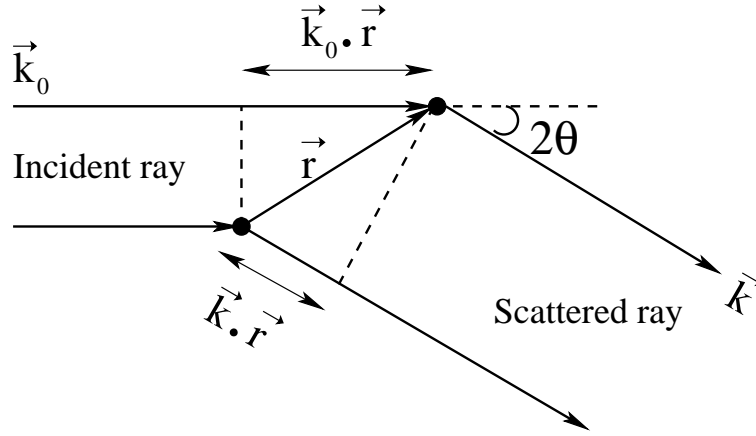


Figure 1.10: Geometric arrangement of scattering event from two scattering centres separated by a distance r .

$$\int \rho(\vec{r})e^{-i\vec{q}\cdot\vec{r}}d\vec{r} = \int \rho_l(\vec{r})e^{-i\vec{q}\cdot\vec{r}}d\vec{r} \int \rho_b(\vec{r})e^{-i\vec{q}\cdot\vec{r}}d\vec{r} = F_l F_b \quad (1.13)$$

where $F_l(q)$ and $F_b(q)$ are the Fourier transforms of the lattice and basis functions, respectively.

From Eq. (1.11) the scattered intensity can be expressed as

$$I(\vec{q}) \sim |F_l(\vec{q})|^2 |F_b(\vec{q})|^2 = S(\vec{q})f(\vec{q}) \quad (1.14)$$

Here $S(\vec{q}) = |F_l(\vec{q})|^2$, called the ‘structure factor’, determines the points in the reciprocal lattice, and $f(\vec{q}) = |F_b(\vec{q})|^2$, the ‘form factor’ determines the intensity at these points.

For an infinite 3-D lattice defined by the crystallographic unit vectors \vec{a} , \vec{b} and \vec{c} , the lattice function will be a 3-D array of δ functions, given by [33],

$$\rho_l(\vec{r}) = \sum_{m,n,p} \delta(\vec{r} - [m\vec{a} + n\vec{b} + p\vec{c}]) \quad (1.15)$$

where m, n and p are integers. The Fourier transform of this function is,

$$F_l(\vec{q}) = \sum_{h,k,l} \delta(\vec{q} - [h\vec{a}^* + k\vec{b}^* + l\vec{c}^*]) \quad (1.16)$$

where a^*, b^* and c^* are the basis vectors in the reciprocal lattice and h, k and l are integers. Finally the scattered intensity can be written as,

$$I(\vec{q}) \sim \frac{1}{(\vec{a} \cdot \vec{b} \times \vec{c})^2} |F_b(\vec{q})|^2 \sum_{h,k,l} \delta(\vec{q} - [h\vec{a}^* + k\vec{b}^* + l\vec{c}^*]) \quad (1.17)$$

From this expression, it can again be seen that the diffraction pattern of an infinite lattice is another infinite 3-D lattice. The position of the diffraction peaks are determined the by the *Miller Indices* (hkl) and their intensities by the values of the ‘form factor’ at these reciprocal lattice points.

1.2.2 Intensity corrections

The calculation of the electron density map from the diffraction data requires the intensities of different reflections to be put on a relative scale. In order to do that certain corrections have to be applied to the observed data. In the case of many lattices more than one equivalent reflection can overlap at the same value of q in the diffraction pattern of an unoriented sample. The observed intensity has to be reduced by a ‘multiplicity’ factor to get the intensity of any one of the overlapping peaks. For example, the peaks corresponding to the indices (10), ($\bar{1}0$), (01), (0 $\bar{1}$), ($\bar{1}1$) and (1 $\bar{1}$) from a 2-D hexagonal lattice will overlap in the diffraction pattern of an unoriented sample. Therefore, we have to reduce the intensity by a multiplicity factor of 6 to obtain the intensity of the (10) peak only.

Another important correction that needs to be applied is the ‘geometric’ correction, which depends both on the type of sample and the geometry of the detector used to collect the data. The scattered intensity corresponding to each peak from an unoriented sample is distributed over a spherical shell of radius q . A 1-D detector, such as a position sensitive detector (PSD) intersects such a shell at two points. The observed intensity has to be multiplied by the area $4\pi q^2$ of the shell in order to get the total intensity. A 2-D detector, such as an image plate, intersects the intensity shell along a plane resulting in a ring. The observed intensities integrated over each ring should be multiplied by the correspond value of q in order to get the total intensity of the peak.

1.2.3 Experimental set up

The experimental set up used for x-ray diffraction studies is shown in figure 1.11. X-rays were produced in a rotating anode generator (Rigaku, UltraX18) operating at 48 KV and 80 mA. A flat

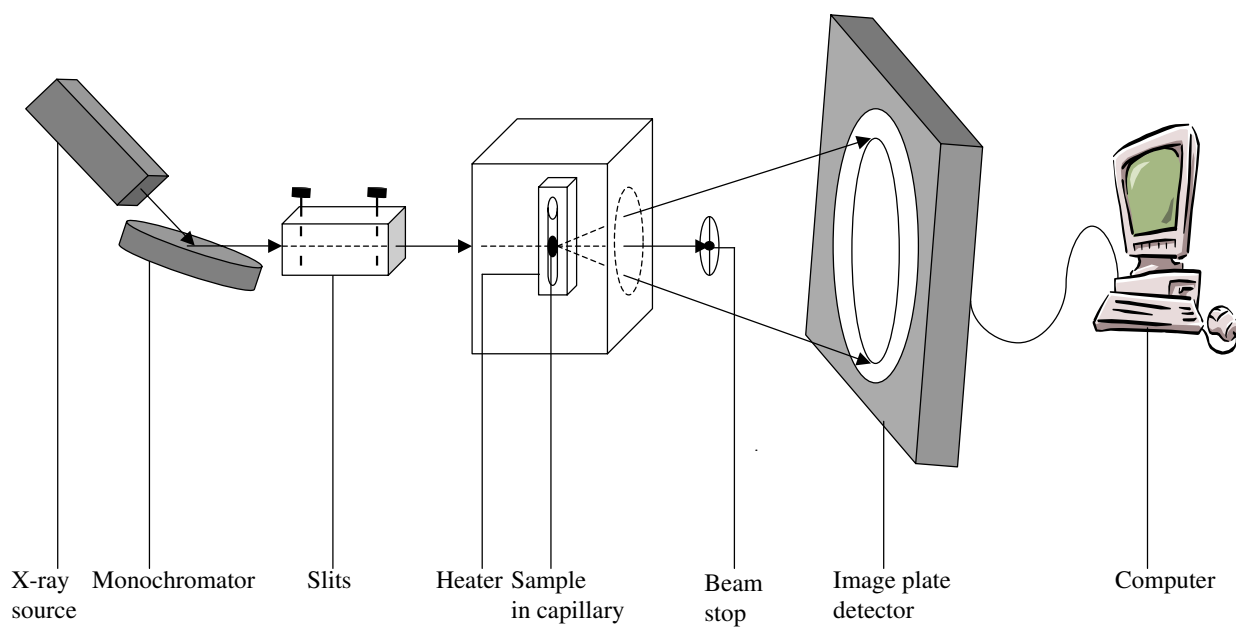


Figure 1.11: Schematic of the experimental set up used for x-ray diffraction study of a powder sample.

graphite monochromator (Huber) was used to select the CuK_{α} radiation of wave length 1.54 \AA . The monochromatic rays pass through a collimator where the beam radius could be tuned with the help of two adjustable slits. Samples were taken in glass capillaries with diameter $\sim 1mm$, and were flame-sealed. Some of the very viscous samples were sucked into glass capillaries of $\sim 0.5mm$ diameter. In this case partially aligned samples were obtained where the surfactant aggregates had a preferential orientation with respect to the capillary axis. The sample was then placed inside a home built heater. The temperature of this heater is controlled by a proportional-integral-derivative (PID) controller programme to an accuracy of $\pm 0.1^{\circ}C$. The x-ray beam was scattered from the sample and the diffraction patterns were recorded on a two dimensional (2-D) image plate (Marresearch) of 80mm diameter. A beam stop made up of lead was placed between the sample and the detector to prevent the very intense direct beam from falling on the detector. The diffraction patterns were scanned and transferred in the form of 16 bit binary data. The exposure time, depending upon the type of sample, was around 1 to 3 hours. Typical sample to detector distance was 250 - 300 mm. The instrumental resolution (full width at half maximum) was 0.18 nm^{-1} . Spacings of the sharp peaks in the diffraction pattern could be measured to an accuracy of $\pm 0.03 \text{ nm}$ whereas the corresponding quantity for the diffuse peaks was $\pm 0.1 \text{ nm}$.

The diffraction pattern from a powder sample consists of concentric rings as shown in figure 1.12. The corresponding separation between various crystallographic planes could be calculated from Bragg's law, $2d\sin\theta = n\lambda$. Here $\theta = \frac{1}{2}\tan^{-1}(\frac{R}{D})$, where R is the radius of the circular ring and D the sample to detector distance. The integrated intensity $I(q)$ was obtained by integrating the diffraction pattern over the azimuthal angle.

1.3 Polarizing optical microscopy

Polarizing optical microscopy (POM) is a technique widely used to identify liquid crystalline phases [34]. Liquid crystalline phases are birefringent. Thin layers of these materials taken between two glass plates exhibit characteristic textures between crossed polarizers under an optical microscope (Fig. 1.13). These textures arise from defects in the medium, which create deformations in the orientational ordering in the medium over length scales of the order of tens of

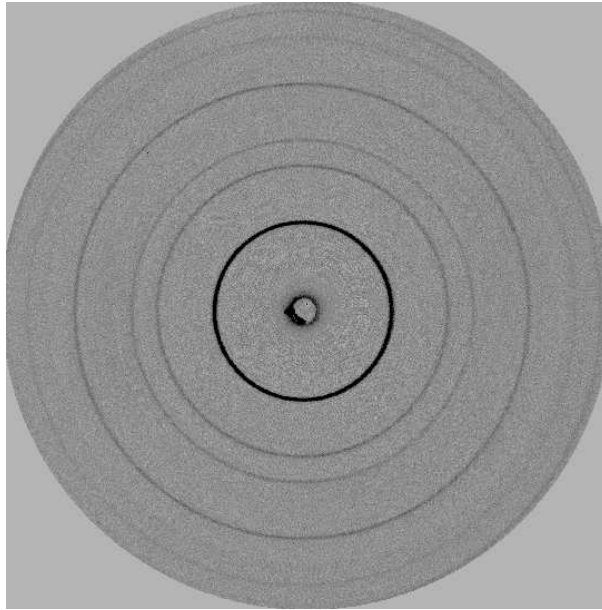


Figure 1.12: Diffraction pattern of a powder sample showing a number of concentric rings collected on a 2-D image plate detector

micrometers due to the low elastic constants of the system. Since the types of defects in a medium are restricted by the symmetry of its structure, the textures resulting from these defects are characteristic of the structure. Hence these textures can be used as ‘fingerprints’ to identify different liquid crystalline phases.

As an example, we shall briefly discuss the defects in a nematic liquid crystal and the textures resulting from them. The nematic phase exhibits long-range orientational ordering of the constituent molecules or micelles, as the case may be. Positional ordering is only short-range, as in the isotropic phase. The orientational ordering in the medium is described in terms of an apolar unit vector, called the ‘director’ (\vec{n}) (Fig. 1.6A). Both point and line defects, called disclinations, are allowed in the director field [6, 34]. The ‘strength’ s of a disclination is defined as the angle, in units of 2π , by which the director rotates along a closed contour surrounding the defect (Fig. 1.14). It can be shown that only $s = \pm 1/2$ lines are stable, and that the point defects correspond to $s = \pm 1$.

A layer of nematic containing point defects and line defects oriented along the line of observation give rise to the ‘Schlieren’ texture (Fig. 1.15) [35]. This texture is obtained when the director field is confined to the plane of the layer, but with no preferred direction of orientation in this plane.

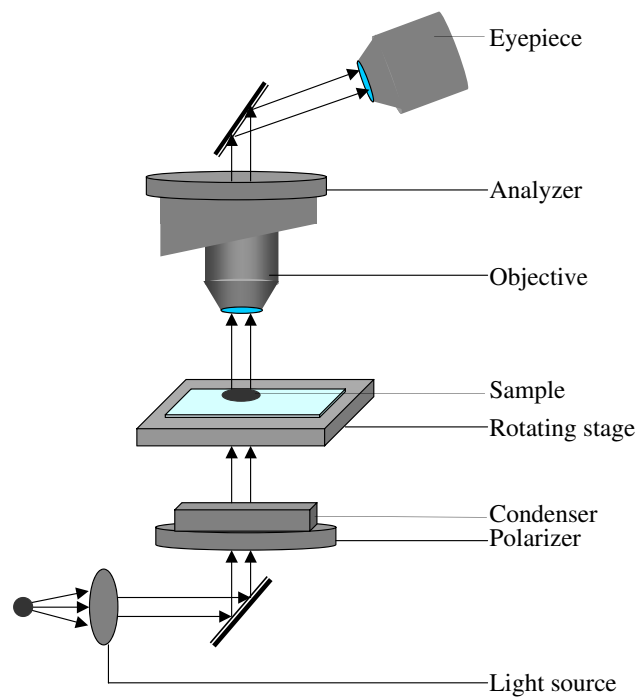


Figure 1.13: Schematic diagram of a polarizing optical microscope.

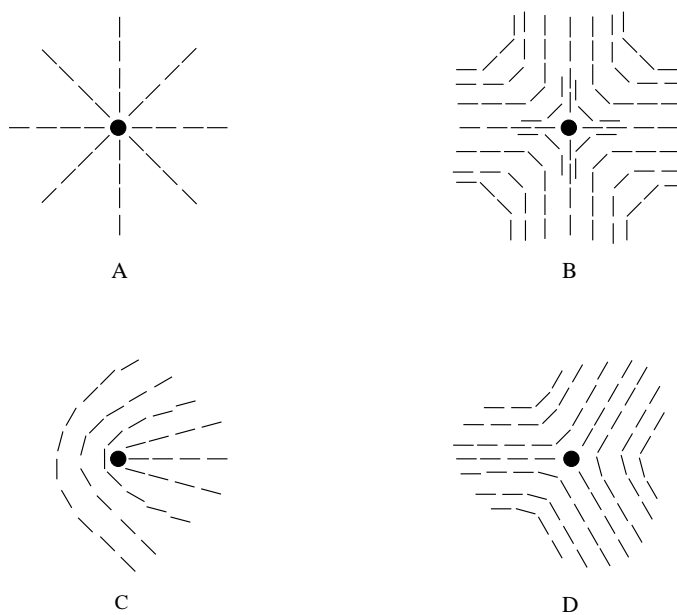


Figure 1.14: Geometrical arrangement of molecules around a point disclination with the strength $s = (A) + 1$, $(B) -1$, $(C) +\frac{1}{2}$ and $(D) -\frac{1}{2}$, respectively.

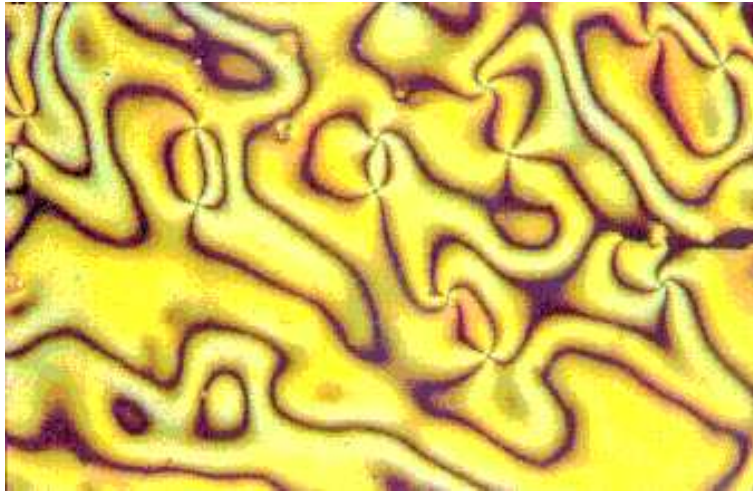


Figure 1.15: Typical ‘Schlieren’ texture of nematic phase [35].

It consists of a network of dark brushes corresponding to regions where the director field is either parallel or normal to one of the crossed polarizers. Four brushes emanate from a disclination of strength 1 and two emanate from a disclination of strength $1/2$. If the disclination lines make a large angle with the direction of observation they give rise to the ‘threaded’ texture. These disclination lines either form closed loops in the medium or end at the surfaces. In fact these thread-like structures are responsible for the name nematic.

If the director field is aligned along the direction of observation the sample would appear uniformly dark. This type of alignment is called ‘homeotropic’ or ‘pseudo-isotropic’. In planar aligned samples the director field is oriented along a preferred direction in the plane of the nematic layer.

1.4 Characterization of lyotropic liquid crystalline phases

In this section we briefly describe the characterization of some of the commonly observed lyotropic liquid crystalline phases using polarizing optical microscopy and x-ray diffraction.

1.4.1 Nematic phase

As we discussed earlier, this phase consists of amphiphilic aggregates of anisotropic shape having long-range orientational ordering and short-range positional ordering (Fig. 1.6A). There are two

types of nematic phases: one is made up of rod-like micelles (N_C) whereas the other has disc-like micelles (N_D). In the N_C phase there is long-range correlation in the orientation of the long axes of the rods, whereas in the N_D phase there is long-range correlation in the orientation of the normal to the discs. Between crossed polarizers this phase exhibits either a schlieren or thread-like texture, which have been discussed in the previous section (Fig. 1.15). The N_D phase can be distinguished from the N_C phase by the presence of large pseudo-isotropic regions due to the preference of the disk-like aggregates to align parallel to the glass substrate. The rod-like micelles of the N_C phase, tend to align with their long axes parallel to the glass substrate, and hence cannot give rise to such homeotropically aligned regions.

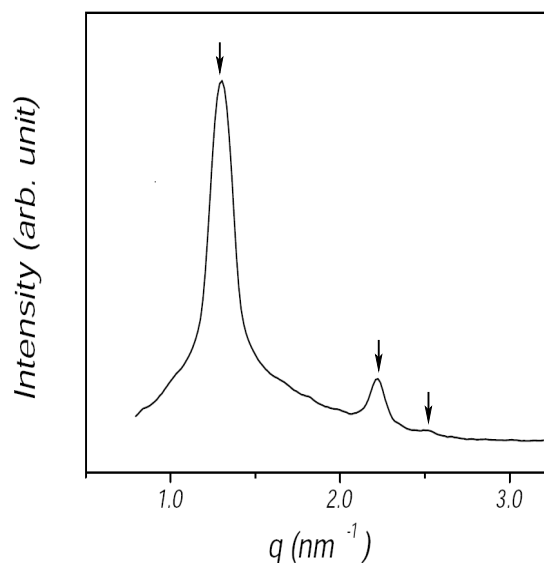
There are two length scales associated with a nematic phase. One corresponds to the ‘face to face’ separation (d_1) of the micelles along the nematic director. The other comes from the ‘side by side’ separation (d_2) in the plane perpendicular to the director. The x-ray scattering experiments of a single domain sample shows two sets of reflections on a 2-D detector which are perpendicular to each other and are related to these two length scales. Both these peaks are broad due to the liquid-like positional order in the system. Such a single domain sample can be prepared by the application of a magnetic field, due to the anisotropy in the diamagnetic susceptibility of the medium. The peak related to separation d_1 is usually sharper than the one corresponding to d_2 in case of a disc like aggregate, due to the longer positional correlation length in the former direction. For a similar reason the peak corresponding to d_2 is usually sharper in the N_C phase; the d_1 peak is usually very broad in these systems due to the highly polydisperse length distribution of the rod-like micelles. The d_2 peak in the case of the N_D phase and the d_1 peak in the case of the N_C phase also occur at much smaller angles, due to the larger dimensions of the two types of aggregates along these directions. Therefore, very often, only the d_1 peak is observed from a N_D phase, and the d_2 from a N_C phase.

1.4.2 Hexagonal phase

This phase consists of long cylindrical aggregates arranged on a 2D hexagonal lattice (Fig. 1.6B). Under polarizing microscope, this phase shows a characteristic smooth texture without any sharp



A



B

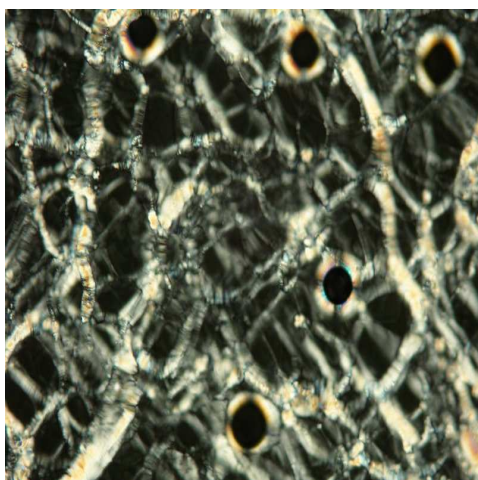
Figure 1.16: Characterization of 2D hexagonal phase: (A) typical texture under crossed polarizers [36] and (B) x-ray diffraction pattern showing three peaks with q in the ratio $1 : \sqrt{3} : 2$.

features (Fig. 1.16A).

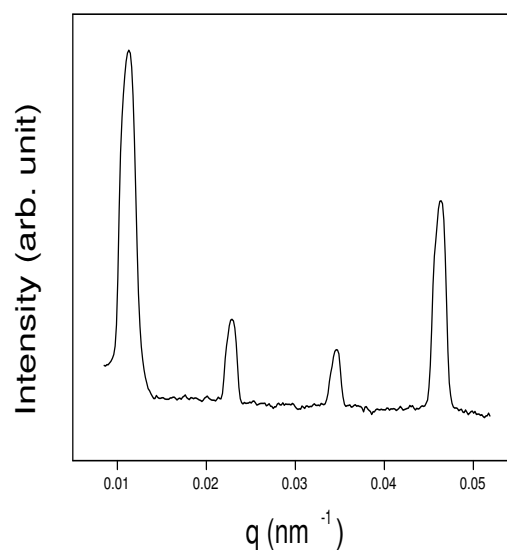
X-ray diffraction patterns show a broad peak in the wide angle region corresponding to the average separation between the molten hydrocarbon chains. In small angle region, the diffraction pattern contains a number of reflections with the magnitude of the scattering vector (q) in the ratio $1 : \sqrt{3} : 2 : \sqrt{7} \dots$ (Fig. 1.16B). These reflections corresponds to the (10), (11), (20), (12). . . planes of a 2-D hexagonal lattice [36].

1.4.3 Lamellar phase

One of the commonly encountered mesophases in lyotropic system is the lamellar phase. It consists of a periodic stack of bilayers separated by water. In the fluid L_α phase the hydrocarbon chains of the amphiphiles are molten and the in-plane order within each bilayer is liquid-like. On the other hand, in the ‘gel’ L_β phase the chains are predominantly in the all-*trans* conformation and are arranged on a 2-D lattice in the plane of the bilayer. The gel phase is usually of interest only in the case of double-chained lipids. Like other anisotropic phases the lamellar phases show very distinct optical textures, reflecting the types of defects occurring in the medium. The most commonly



A



B

Figure 1.17: Characterization of lamellar phase: (A) ‘oily streak’ texture and (B) x-ray diffraction pattern showing four peaks with q in the ratio 1 : 2 : 3 : 4.

observed one is the focal conic texture. In the case of dilute lamellar phases the bilayers have a strong tendency to orient parallel to the bounding surfaces. This leads to large pseudo-isotropic regions in the texture, where the optic axis, which is along the bilayer normal, is oriented along the direction of observation. In this case an ‘oily streak’ texture is obtained consisting of birefringent streaks separating dark regions (Fig. 1.17A). When a lamellar phase coexists with excess water, the bilayers normally curl up into multilamellar vesicles. Such systems exhibit a characteristic ‘Maltese cross’ texture.

Since the lamellar phase is a 1-D crystal, its diffraction pattern consists of a set of reflections in the small angle region, with their q values in the ratio 1 : 2 : 3 : 4, etc (Fig. 1.17B). The lamellar periodicity d , which is the sum of the thicknesses of the bilayer and water layer, can be directly obtained using $d = 2\pi/q_0$, where q_0 is the position of the first peak. The L_α phase gives a broad wide angle peak, corresponding to the average separation between the chains. Sharper wide angle reflections are obtained in the case of the L_β phase, arising from the 2D chain lattice.

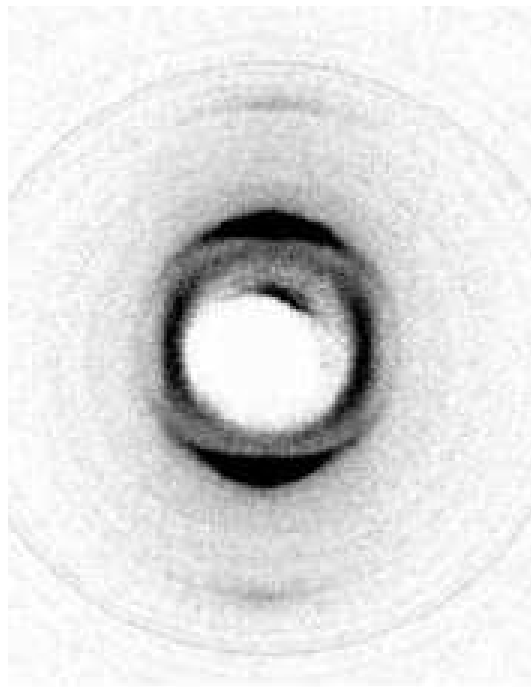
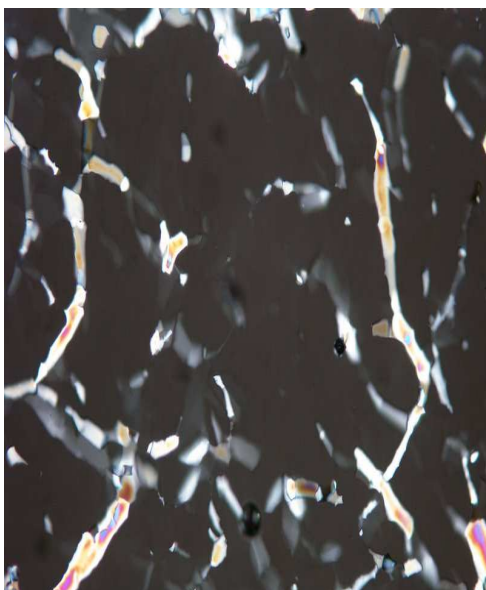


Figure 1.18: Diffraction pattern of a random mesh phase. The horizontal diffuse spots arise from structural inhomogeneities in the amphiphilic bilayers [37].

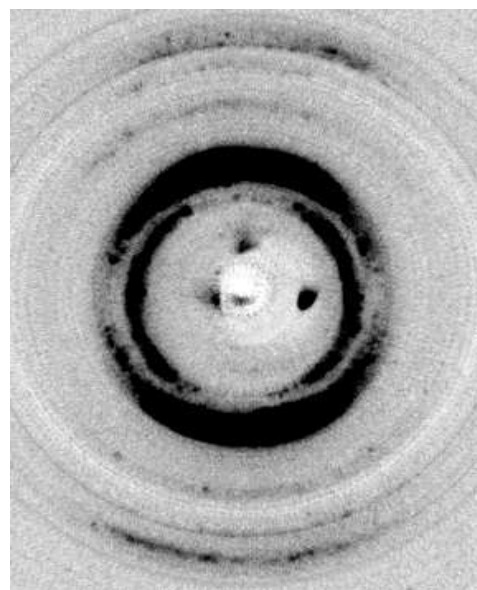
1.4.4 Intermediate phases

Intermediate phases in lyotropic liquid crystalline systems are the topological intermediaries between the hexagonal and lamellar phases. Various phases observed at these compositions have been discussed in section 1.3. Here we shall discuss the experimental identification of random and ordered mesh phases and also of bicontinuous cubic phases which we will come across in different chapters of this thesis.

The random mesh phase is essentially a lamellar phase, but contains water filled curvature defects in the plane of the bilayer. These defects have short-range positional correlation in the plane of the bilayer, but are uncorrelated across bilayers. Due to their lamellar structure, they show textures similar to those of regular lamellar phases with continuous bilayers. The presence of the defects can be deduced from diffraction experiments, which show a diffuse peak in the small angle region in addition to the lamellar peaks. Diffraction patterns of oriented samples show that the diffuse peak is in a direction normal to the direction of the lamellar peaks, indicating that it arises from structural inhomogeneities in the plane of the bilayer (Fig. 1.18). In the intermediate



A



B

Figure 1.19: Characterization of ordered mesh phase: (A) ‘mosaic texture’ along with ‘homeotropic’ region and (B) x-ray diffraction pattern showing many reflections that can be indexed on a 3D lattice.

mesh phase these defects get locked into a 3-D lattice. The microscopy texture of this phase is different from that of the random mesh phase, reflecting the change in the symmetry of the system. The typical texture observed is a ‘mosaic’ one, which often contains pseudo-isotropic regions (Fig. 1.19A). The diffraction pattern of the ordered mesh phase consists of many reflections corresponding to the 3-D structure of the system (Fig. 1.19B). From the positions of these peaks the structure of the phase can be deduced. Most of the ordered mesh phases reported in the literature have either a tetragonal or a hexagonal structure.

Cubic phases are optically isotropic and hence look dark under crossed polarizers. X-ray diffraction patterns of these phases show a number of sharp peaks which can be indexed on a cubic lattice. From the systematic absence of certain reflections, the space group symmetry of the structure can often be deduced. For example, the diffraction pattern shown in figure 1.20 corresponds to the space group $Pn3m$.

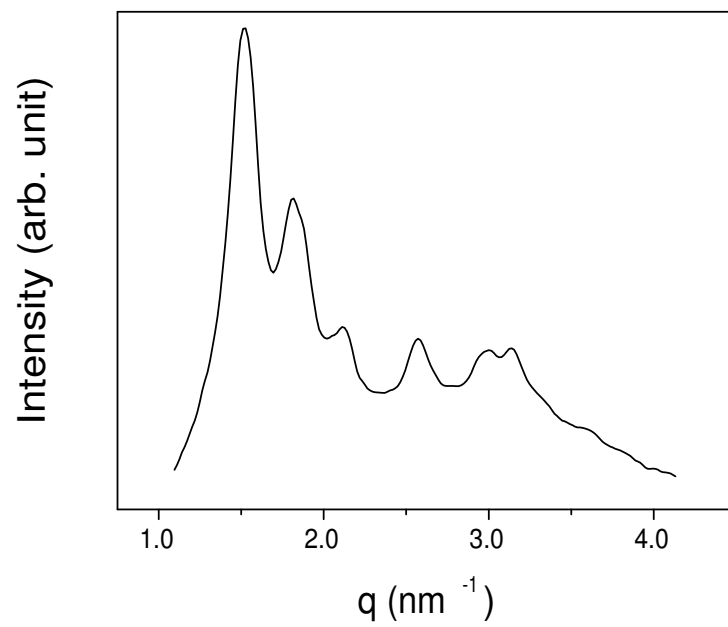


Figure 1.20: Diffraction pattern of a bicontinuous cubic phase corresponding to the space group $Pn3m$.

Bibliography

- [1] J. Israelachvili *Intermolecular and Surface Forces*, 2nd edition, Academic Press, London (1991).
- [2] C. Tanford *The Hydrophobic Effect*, 2nd edition, Wiley, New York (1980).
- [3] A. Ben-Shaul and W. M. Gelbart in *Micelles, Membranes, Microemulsions and Monolayers*, Eds. W. M. Gelbert, A. Ben-Shaul and D. Roux, Springer-Verlag, New York (1994).
- [4] E. M. Landau and J. P. Rosenbusch *Proc. Natl. Acad. Sci. USA*, **93**, 14532 (1996).
- [5] R. J. Hunter *Foundations of Colloid Science*, Oxford University Press, USA (1987).
- [6] P. G. de Gennes and J. Prost *The Physics of Liquid Crystal*, 2nd edition, Oxford University Press, Oxford (1994).
- [7] L. Coppola, R. Gianferri, I. Nocotera, C. Oliviero and G. A. Ranieri *Phys. Chem. Chem. Phys.*, **6**, 2364 (2004).
- [8] G. Lindblom and L. Rilfors *Biochem. Biophys. Acta*, **988**, 221 (1989).
- [9] K. Fontell *Adv. Colloid Interface Sci.*, **41**, 127 (1992).
- [10] *Bicontinuous Liquid Crystal*, Eds. M. L. Lynch and P. T. Spicer, Taylor & Francis, Boca Raton, (2005).
- [11] P. Kekicheff *J. Colloid Interface Sci.*, **131**, 133 (1989).
- [12] S. S. Funari, M. C. Holmes and G. J. T. Tiddy *J. Phys. Chem.*, **96**, 11029 (1992).

- [13] S. S. Funari and G. Rapp *Proc. Natl. Acad. Sci. USA*, **96**, 7756 (1999).
- [14] S. T. Hyde *J. Physique (Coll.)*, **C-7**, 209 (1990).
- [15] S. T. Hyde *Colloid Surfaces A: Physicochem. Eng. Aspects*, **103**, 227 (1995).
- [16] K. Rendall and G. J. T. Tiddy *J. Chem. Soc., Faraday Trans. 1*, **80**, 3339 (1984).
- [17] S. S. Funari, M. C. Holmes and G. J. T. Tiddy *J. Phys. Chem.*, **98**, 3015 (1994).
- [18] J. Burgoyne, M. C. Holmes and G. J. T. Tiddy *J. Phys. Chem*, **99**, 6054 (1995).
- [19] P. Strom and D. M. Anderson *Langmuir*, **8**, 691 (1992).
- [20] R. Bandyopadhyay and A. K. Sood *Langmuir*, **19**, 3121 (2003).
- [21] R. Gomati, J. Appell, P. Bassereau, J. Marignan and G. Porte *J. Phys. Chem*, **91**, 6203 (1987).
- [22] M. E. Cates and S. J. Candau *J. Phys.: Condens Matter*, **2**, 6869 (1996).
- [23] P. A. Hassan, S. R. Raghavan and E. W. Kaler *Langmuir* **18**, 2543 (2002).
- [24] B. K. Mishra, S. D. Samant, P. Pradhan, S. B. Mishra and C. Manohar *Langmuir* **9**, 894 (1993).
- [25] E. H. Lucassen-Reynders, J. Lucassen and D. Giles *J. Colloid Interface Sci.* **81**, 150 (1981).
- [26] E. W. Kaler, K. L. Herrington, A. K. Murthy, and J. A. N. Zasadzinski *J. Phys. chem.* **96**, 6698 (1992).
- [27] K. L. Herrington, E. W. Kaler, D. D. Millar, J. A. Zasadzinski and S. Chiruvolu *J. Phys Chem.* **97**, 13792 (1993).
- [28] M. J. Blandamer, B. Briggs, P. M. Cullis and B. F. N Engberts *Phys. Chem. Chem. Phys.* **2**, 5146 (2000).
- [29] H. I. Petrache, T. Zemb, L. Belloni and V. A. Parsegian *Proc. Natl. Acad. Sci. USA*, **103**, 7982 (2006).

- [30] R. Schomacker and R. Strey *J. Phys. Chem.* **98**, 3908 (1994).
- [31] B. E. Warren, *X-ray diffraction*, Dover Publications, New York (1990).
- [32] D. C. Champeney *Fourier Transforms and Their Physical Applications*, Academic Press, London (1973).
- [33] D. Sherwood, *Crystal, X-rays and Protein*, Longman, London (1976).
- [34] P. J. Collings and M. Hird *Introduction to Liquid Crystals Chemistry and Physics*, Taylor & Francis, Bristol (1997).
- [35] <http://people.ccmr.cornell.edu/cober/mse124/nematic-hilmar.gif>
- [36] S. T. Hyde in *Handbook of Applied Surface and Colloid Chemistry*, Eds. Krister Holmberg, John Wiley & Sons (2001).
- [37] R. Krishnaswamy, S. K. Ghosh, S. Laksmanan, V. A. Raghunathan and A. K. Sood *Langmuir* **21**, 10439 (1998).